Influence of the size and curvedness of neural projections on the orientationally averaged diffusion MR signal

Evren Özarslan [1,2,*], **Cem Yolcu** [1], **Magnus Herberthson** [3], **Hans Knutsson** [1] **and Carl-Fredrik Westin** [1,3]

[1] *Department of Biomedical Engineering, Linköping University, Linköping, Sweden*
[2] *Center for Medical Image Science and Visualization, Linköping University, Linköping, Sweden*
[3] *Division of Mathematics and Applied Mathematics, Department of Mathematics, Linköping University, Linköping, Sweden*
[4] *Laboratory for Mathematics in Imaging, Department of Radiology, Brigham and Women's Hospital, Harvard Medical School, Boston, MA, USA*

Correspondence*:
Linköpings universitet
Campus US
Institutionen för medicinsk teknik
581 85 Linköping Sweden
evren.ozarslan@liu.se

Citation:
Özarslan E, Yolcu C, Herberthson M, Knutsson H and Westin CF (2018)
Influence of the Size and Curvedness of Neural Projections on the Orientationally Averaged Diffusion MR Signal
Front. Phys. 6:17
doi:10.3389/fphy.2018.00017

APPENDIX A: DERIVATIONS FOR THE SIGNAL DECAY TENSORS

Here, we provide the derivations of the signal decay tensors, $\boldsymbol{V}$, for regimes A, B, and C, respectively. Fig. 5 illustrates the decay tensors as ellipses for an examplary selection of planar curves.

Regime A and $D\Delta \ll R_c^2$

For small values of $q^2 D\Delta$, the exponent in (3) is small, so the expression can be rewritten to leading order, by moving the averaging integral into the exponent, as

$$E(\boldsymbol{q}) \approx e^{-D\Delta \frac{1}{\ell} \int_0^\ell \mathrm{d}s\, \boldsymbol{q}^\intercal \hat{\boldsymbol{t}}(s) \hat{\boldsymbol{t}}^\intercal(s) \boldsymbol{q}} \,. \tag{20}$$

In this small-q regime, the form $E(\boldsymbol{q}) = e^{-\boldsymbol{q}^\intercal \boldsymbol{V} \boldsymbol{q}}$ (1) identifies the decay tensor V_{ij} as

$$V_{ij} = \frac{D\Delta}{\ell} \int_0^\ell \mathrm{d}s\, \frac{\mathrm{d}r_i(s)}{\mathrm{d}s} \frac{\mathrm{d}r_j(s)}{\mathrm{d}s} \,. \tag{21}$$

The integrand in the above expression is a rank-1 tensor by construction. For a general curve, the integral mixes together different rank-1 tensors resulting in a V_{ij} of higher rank, the only exception being a straight line. Note that since $\mathrm{d}\boldsymbol{r}/\mathrm{d}s$ is a unit vector, the trace of the above matrix is $D\Delta$. The orientationally-averaged signal (2) in the small $q^2 D\Delta$ regime is just $\bar{E}(q) \approx e^{-q^2 \operatorname{Tr} \boldsymbol{V}/3} = e^{-q^2 D\Delta/3}$.

Regime B

The three-dimensional Fourier transform of the spin density (13) is given by

$$\tilde{\rho}(\boldsymbol{q}) = \frac{1}{\ell} \int_0^\ell \mathrm{d}s\, e^{-i\boldsymbol{q}\cdot\boldsymbol{r}(s)} \,, \tag{22}$$

which is substituted into $E(\boldsymbol{q}) = |\tilde{\rho}(\boldsymbol{q})|^2$, yielding the signal decay

$$E(\boldsymbol{q}) = \frac{1}{\ell^2} \int_0^\ell \mathrm{d}s \int_0^\ell \mathrm{d}s'\, e^{-i\boldsymbol{q}\cdot[\boldsymbol{R}(s) - \boldsymbol{R}(s')]} \,. \tag{23}$$

In this expression, we employed the change of variables $\boldsymbol{R}(s) = \boldsymbol{r}(s) - \boldsymbol{R}_{\mathrm{cm}}$, where $\boldsymbol{R}_{\mathrm{cm}}$ is the center of mass of the curve. For small q values, the exponential can be replaced by its Maclaurin series up to quadratic order. Term-by-term evaluation of the double integral then yields

$$\begin{aligned} E(\boldsymbol{q}) &\approx 1 - \frac{1}{\ell} \int_0^\ell \mathrm{d}s\, [\boldsymbol{q}\cdot\boldsymbol{R}(s)]^2 \\ &\approx \exp\left(-\frac{1}{\ell} \int_0^\ell \mathrm{d}s\, \boldsymbol{q}^\intercal \boldsymbol{R}(s) \boldsymbol{R}(s)^\intercal \boldsymbol{q} \right) \,, \end{aligned} \tag{24}$$

which leads to the identification of the signal decay tensor given by

$$V_{ij} = \frac{1}{\ell} \int_0^\ell \mathrm{d}s\, R_i(s)\, R_j(s) \,. \tag{25}$$

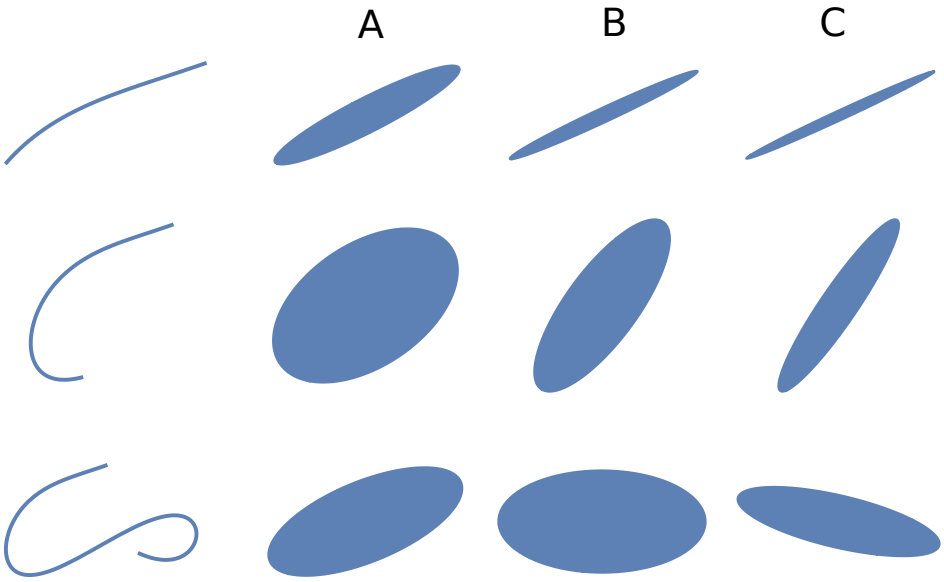

Figure 5. Figure showing three planar curves (left column), and ellipses depicting the signal decay tensor in the three regimes A, B, and C (see equations (21), (25), and (19)) considered. Here, the ellipses for the tensors were rescaled so as to produce a depiction of the same size.

Like in the previous regime, V_{ij} is rank-1 only for straight fibers. The trace of the above matrix is $R_{\rm g}^2$, by definition. The orientationally-averaged signal (2) in the small $qR_{\rm g}$ regime is then just $\bar{E}(q) \approx e^{-q^2 \,{\rm Tr}\, \boldsymbol{V}/3} = e^{-(qR_{\rm g})^2/3}$.

Regime C

Similar to regime B, the signal decay tensor V_{ij} is the variance of a probability distribution; this time the center of mass distribution, $p_{\rm cm}(\boldsymbol{\xi}, \delta)$. Using the definition (16), the variance $\langle \xi_i \xi_j \rangle - \langle \xi_i \rangle \langle \xi_j \rangle$ can be calculated as

$$V_{ij} = \frac{2}{\ell \delta^2} \int_0^\delta {\rm d}t_1 \int_{t_1}^\delta {\rm d}t_2 \int_0^\ell {\rm d}s_1 \int_0^\ell {\rm d}s_2 \, r_i(s_1) r_j(s_2) \left[P(s_2, t_2 | s_1, t_1) - \frac{1}{\ell} \right] , \tag{26}$$

where [65]

$$P(s, t' + t | s', t') = \frac{1}{\ell} + \frac{2}{\ell} \sum_{n=1}^\infty e^{-\frac{n^2 \pi^2 D t}{\ell^2}} \cos \frac{n\pi s}{\ell} \cos \frac{n \pi s'}{\ell} \tag{27}$$

is the propagator from arc-length coordinate s' to s in a time t. The time integrals in (26) are done easily, and after further dropping exponentially decaying temporal terms on account of $D\delta \gg \ell^2$, one obtains

$$V_{ij} = \frac{4}{\pi^2 D \delta} \int_0^\ell {\rm d}s_1 \int_0^\ell {\rm d}s_2 \sum_{n=1}^\infty \left(\frac{1}{n^2} - \frac{\ell^2}{\pi^2 n^4 D \delta} \right) \cos \frac{n \pi s_1}{\ell} \cos \frac{n \pi s_2}{\ell} \, . \tag{28}$$

It turns out that the sum over n admits a closed form, which results in the final expression (19).

APPENDIX B: COMPUTING THE SIGNAL FOR DIFFUSION ON A CIRCLE

We employed the multiple correlation function (MCF) framework [66, 67, 68, 69] for estimating the signal attenuation due to diffusion taking place on a circle whose radius is denoted by R. This problem can be considered as the limiting case of the problem involving diffusion within circular layers of finite thickness [70].

The evolution of magnetization is governed by the Bloch-Torrey equation [71]. For our problem, it can be written as

$$\frac{\partial M}{\partial t} = \frac{D}{R^2}\frac{\partial^2 M}{\partial \phi^2} - i\gamma R G(t)\cos\phi M(\phi,t)\ , \tag{29}$$

where we assumed that the gradients are applied along the x direction. The MCF approach considers the eigenproblem

$$\frac{\partial^2 u_k(\phi)}{\partial \phi^2} = -\lambda_k u_k(\phi) \tag{30}$$

along with the periodicity condition $u_k(\phi + 2\pi) = u_k(\phi)$, which is valid for the circular geometry. The eigenvalues are simply k^2, while the eigenfunctions are $u_k(\phi) = (2\pi)^{-1/2}e^{ik\phi}$, where k is any integer.

The MCF technique is based on expressing the problem of computing the signal attenuation in this eigenbasis. The two terms on the right hand side of (29) lead to two infinite-dimensional matrix operators, which we shall denote by $\mathbf{\Lambda}$ and $\boldsymbol{A}$, respectively. The components of these operators are given by

$$\Lambda_{m,n} = n^2\delta_{m,n}\ , \text{and} \tag{31}$$

$$A_{m,n} = \frac{1}{2}(\delta_{m,n+1} + \delta_{m,n-1})\ . \tag{32}$$

The signal for a Stejskal-Tanner measurement is given simply by the element of the matrix

$$e^{-\mathbf{\Lambda}D\delta/R^2 - iqR\boldsymbol{A}}e^{-\mathbf{\Lambda}D(\Delta-\delta)/R^2}e^{-\mathbf{\Lambda}D\delta/R^2 + iqR\boldsymbol{A}} \tag{33}$$

identified by the indices 0 and 0.

APPENDIX C: ON THE DEBYE-POROD LAW

For a bipolar pulsed gradient sequence, the signal $E(\boldsymbol{q})$ is the Fourier transform of a displacement probability distribution, $P(\boldsymbol{r})$, often referred to as the average propagator (between center of mass positions if pulses are of long duration [40]). When the specimen is macroscopically isotropic, *e.g.*, if it consists of a uniform orientational distribution of identical compartments, the signal becomes

$$\bar{E}(q) = 4\pi\int_0^\infty \mathrm{d}r\, r^2\frac{\sin(qr)}{qr}\bar{P}(r)\ , \tag{34}$$

using the purely radial term in the spherical wave expansion of $e^{-i\boldsymbol{q}\cdot\boldsymbol{r}}$, where $\bar{P}(r) = (4\pi)^{-1}\int \mathrm{d}\Omega\, P(\boldsymbol{r})$ is the orientational average of $P(\boldsymbol{r})$. In the physics of scattering, this formula is identical to that of

the scattered intensity originating from a dilute aggregation of randomly-oriented scatterers, with $P(\boldsymbol{r})$ identified as the auto-correlation function of the scattering density in proper units [37, 38].

Depending on the analytical properties of the function $\bar{P}(r)$, it may be possible to develop the signal (34) into an asymptotic expansion in powers of q^{-1}. This is achieved by repeated integrations by parts, exploiting the trivial integral of the sine (or cosine) in the integrand, each repetition yielding (possibly) a term proportional to the next power of q^{-1}. For diffusion in a finite 3D compartment, this procedure is permissible and yields a leading term $\sim q^{-4}$ as $q \to \infty$, whose coefficient was shown to be related to the return-to-origin probability at the surface [27], which is a generalization of what is known as the Debye-Porod law in the field of scattering [37, 38]. This particular exponent of -4 is expected universally, when the measurement is done with a resolution ($\sim q^{-1}$) substantially finer than the smallest dimension of the compartment. Below this cutoff, the compartment will appear effectively lower dimensional, and $\bar{E}(q)$ may exhibit an appreciable stretch of q-values where it exhibits a slower power law decay, depending on the geometry. This is not in conflict with the Debye-Porod law, but simply outside its domain of applicability.

For lower dimensional objects, specific examples of rod and flat disk geometries indicate that $\bar{P}$ is of lower regularity. This means that the procedure of repeated integrations by parts either stops earlier or is even not applicable at all. As a consequence, the leading powers of q in the asymptotic expansion will not be -4, and for the 1D and 2D cases, [37], these leading powers were indeed found to be -1 and -2, respectively.

Gaussian pores

Given how universal the Debye-Porod law is, it may appear contradictory that the orientationally averaged signal (2) arising from 3D Gaussian compartments does not exhibit a q^{-4} decay, but rather a power q^{-1} modulated by a decaying (quadratic) exponential.

To understand this, it is useful to consider more explicitly the asymptotic expansion of the signal (34), rearranged here slightly as,

$$\bar{E}(q) = \frac{4\pi}{q} \int_0^\infty \mathrm{d}r \, \sin(qr) r \bar{P}(r) \, . \tag{35}$$

As mentioned earlier, the asymptotic expansion procedure via integration by parts relies (to a certain extent) on the smoothness of the function $\bar{P}(r)$. In the Gaussian case where the displacement distribution $P(\boldsymbol{r}) \propto e^{-\frac{1}{2}\boldsymbol{r}^\intercal \boldsymbol{V}^{-1}\boldsymbol{r}}$, the orientational average $\bar{P}(r)$ has the same form as (2), but with different variables:

$$\bar{P}(r) \propto r^{-1} e^{-k_0^2 r^2} \mathrm{erf}(k_1 r) \, . \tag{36}$$

Thus, the natural extension (to the space of real numbers $\mathbb{R}$) of $r\bar{P}(r)$ is a smooth odd function which, together with all its derivatives, vanish at infinity. Repeated partial integration of (35) shows that for any even N,

$$\bar{E}(q) = \frac{4\pi}{q^2} \sum_{n=0}^{N/2} \left(\frac{-1}{q^2}\right)^n \frac{\mathrm{d}^{2n}}{\mathrm{d}r^{2n}} \left[r\bar{P}(r)\right] \Big|_{r=0} + \frac{(-1)^{N/2}}{q^{N+2}} \int_0^\infty \mathrm{d}r \cos(qr) \frac{\mathrm{d}^{N+1}}{\mathrm{d}r^{N+1}} \left[r\bar{P}(r)\right] \, . \tag{37}$$

But since $r\bar{P}(r)$ is odd, all even derivatives vanish at $r = 0$. Hence, for any even N,

$$|\bar{E}(q)| \leq \frac{1}{q^{N+2}} \int_0^\infty \mathrm{d}r \left| \cos(qr) \frac{\mathrm{d}^{N+1}}{\mathrm{d}r^{N+1}} \left[r\bar{P}(r)\right] \right| \leq \frac{C_N}{q^{N+2}} \tag{38}$$

for some constant C_N. This means that $\bar{E}(q)$ decays faster than any polynomial[6]. This observation implies that for truly Gaussian compartments [73] or long pulse acquisitions [43] (regime C), the asymptotic decay of $\bar{E}(q)$ should be faster than any polynomial, which is indeed true for the expression in Eq. (2).

REFERENCES

[1] McKinnon ET, Jensen JH, Glenn GR, Helpern JA. Dependence on b-value of the direction-averaged diffusion-weighted imaging signal in brain. *Magn Reson Imaging* **36** (2017) 121–127. doi:10.1016/j.mri.2016.10.026.

[2] Assaf Y, Freidlin RZ, Rohde GK, Basser PJ. New modeling and experimental framework to characterize hindered and restricted water diffusion in brain white matter. *Magn Reson Med* **52** (2004) 965–978.

[3] Stanisz GJ, Szafer A, Wright GA, Henkelman RM. An analytical model of restricted diffusion in bovine optic nerve. *Magn Reson Med* **37** (1997) 103–111.

[4] Jespersen SN, Kroenke CD, Østergaard L, Ackerman JJH, Yablonskiy DA. Modeling dendrite density from magnetic resonance diffusion measurements. *NeuroImage* **34** (2007) 1473–86. doi:10.1016/j.neuroimage.2006.10.037.

[5] Behrens TEJ, Woolrich MW, Jenkinson M, Johansen-Berg H, Nunes RG, Clare S, et al. Characterization and propagation of uncertainty in diffusion-weighted MR imaging. *Magn Reson Med* **50** (2003) 1077–88. doi:10.1002/mrm.10609.

[6] Kroenke CD, Ackerman JJH, Yablonskiy DA. On the nature of the NAA diffusion attenuated MR signal in the central nervous system. *Magn Reson Med* **52** (2004) 1052–9. doi:10.1002/mrm.20260.

[7] Zhang H, Schneider T, Wheeler-Kingshott CA, Alexander DC. NODDI: practical in vivo neurite orientation dispersion and density imaging of the human brain. *NeuroImage* **61** (2012) 1000–16. doi:10.1016/j.neuroimage.2012.03.072.

[8] Stejskal EO, Tanner JE. Spin diffusion measurements: Spin echoes in the presence of a time-dependent field gradient. *J Chem Phys* **42** (1965) 288–292.

[9] Jensen JH. Sufficiency of diffusion tensor in characterizing the diffusion MRI signal to leading order in diffusion weighting. *NMR Biomed* **27** (2014) 1005–1007. doi:10.1002/nbm.3145.

[10] Özarslan E, Basser PJ. Microscopic anisotropy revealed by NMR double pulsed field gradient experiments with arbitrary timing parameters. *J Chem Phys* **128** (2008) 154511. doi:10.1063/1.2905765.

[11] Özarslan E, Koay CG, Shepherd TM, Komlosh ME, İrfanoğlu MO, Pierpaoli C, et al. Mean apparent propagator (MAP) MRI: a novel diffusion imaging method for mapping tissue microstructure. *NeuroImage* **78** (2013) 16–32. doi:10.1016/j.neuroimage.2013.04.016.

[12] Kaden E, Kruggel F, Alexander DC. Quantitative mapping of the per-axon diffusion coefficients in brain white matter. *Magn Reson Med* **75** (2016) 1752–63. doi:10.1002/mrm.25734.

[13] Szczepankiewicz F, Westin CF, Knutsson H. A measurement weighting scheme for optimal powder average estimation. *Proc Intl Soc Mag Reson Med* (2017), vol. 26, 3345.

[14] Mori S, van Zijl PC. Diffusion weighting by the trace of the diffusion tensor within a single scan. *Magn Reson Med* **33** (1995) 41–52.

[15] Wong EC, Cox RW, Song AW. Optimized isotropic diffusion weighting. *Magn Reson Med* **34** (1995) 139–43.

[6] By the extension of $r\bar{P}(r)$ mentioned above, it is clear that $r\bar{P}(r)$ lies in the Schwartz space $S(\mathbb{R})$ [72]. But then (35) is the Fourier transform of $r\bar{P}(r)$ (up to a factor of $-i2\pi q^{-1}$), and since the Fourier transform is an automorphism of $S(\mathbb{R})$, the fall off property of $\bar{E}(q)$ is immediate.

[16] Eriksson S, Lasič S, Topgaard D. Isotropic diffusion weighting in PGSE NMR by magic-angle spinning of the q-vector. *J Magn Reson* **226** (2013) 13–18. doi:10.1016/j.jmr.2012.10.015.

[17] Westin CF, Knutsson H, Pasternak O, Szczepankiewicz F, Özarslan E, van Westen D, et al. Q-space trajectory imaging for multidimensional diffusion MRI of the human brain. *NeuroImage* **135** (2016) 345–62. doi:10.1016/j.neuroimage.2016.02.039.

[18] Lampinen B, Szczepankiewicz F, Mørtensson J, van Westen D, Sundgren PC, Nilsson M. Neurite density imaging versus imaging of microscopic anisotropy in diffusion MRI: A model comparison using spherical tensor encoding. *NeuroImage* **147** (2017) 517–531. doi:10.1016/j.neuroimage.2016.11.053.

[19] Özarslan E. Compartment shape anisotropy (CSA) revealed by double pulsed field gradient MR. *J Magn Reson* **199** (2009) 56–67. doi:10.1016/j.jmr.2009.04.002.

[20] Lawrenz M, Finsterbusch J. Double-wave-vector diffusion-weighted imaging reveals microscopic diffusion anisotropy in the living human brain. *Magn Reson Med* **69** (2013) 1072–1082. doi:10.1002/mrm.24347.

[21] Yablonskiy DA, Sukstanskii AL, Leawoods JC, Gierada DS, Bretthorst GL, Lefrak SS, et al. Quantitative in vivo assessment of lung microstructure at the alveolar level with hyperpolarized ^{3}He diffusion MRI. *Proc Natl Acad Sci U S A* **99** (2002) 3111–6. doi:10.1073/pnas.052594699.

[22] Anderson AW. Measurement of fiber orientation distributions using high angular resolution diffusion imaging. *Magn Reson Med* **54** (2005) 1194–1206. doi:10.1002/mrm.20667.

[23] Veraart J, Fieremans E, Novikov DS. Universal power-law scaling of water diffusion in human brain defines what we see with MRI. *arXiv* (2016) 1609.09145.

[24] Köpf M, Corinth C, Haferkamp O, Nonnenmacher TF. Anomalous diffusion of water in biological tissues. *Biophys J* **70** (1996) 2950–2958.

[25] Yablonskiy DA, Bretthorst GL, Ackerman JJH. Statistical model for diffusion attenuated MR signal. *Magn Reson Med* **50** (2003) 664–9. doi:10.1002/mrm.10578.

[26] Jian B, Vemuri BC, Özarslan E, Carney PR, Mareci TH. A novel tensor distribution model for the diffusion-weighted MR signal. *NeuroImage* **37** (2007) 164–176. doi:10.1016/j.neuroimage.2007.03.074.

[27] Sen PN, Hürlimann MD, de Swiet TM. Debye-Porod law of diffraction for diffusion in porous media. *Phys Rev B* **51** (1995) 601–604.

[28] Özarslan E, Koay CG, Basser PJ. Remarks on q-space MR propagator in partially restricted, axially-symmetric, and isotropic environments. *Magn Reson Imaging* **27** (2009) 834–844. doi:10.1016/j.mri.2009.01.005.

[29] Nørhøj Jespersen S, Buhl N. The displacement correlation tensor: microstructure, ensemble anisotropy and curving fibers. *J Magn Reson* **208** (2011) 34–43. doi:10.1016/j.jmr.2010.10.003.

[30] Nilsson M, Lätt J, Støahlberg F, van Westen D, Hagslätt H. The importance of axonal undulation in diffusion MR measurements: a Monte Carlo simulation study. *NMR Biomed* **25** (2012) 795–805. doi:10.1002/nbm.1795.

[31] Reisert M, Kellner E, Kiselev VG. About the geometry of asymmetric fiber orientation distributions. *IEEE Trans Med Imaging* **31** (2012) 1240–9. doi:10.1109/TMI.2012.2187916.

[32] Pizzolato M, Wassermann D, Boutelier T, Deriche R. Exploiting the phase in diffusion MRI for microstructure recovery: Towards axonal tortuosity via asymmetric diffusion processes. *International Conference on Medical Image Computing and Computer-Assisted Intervention* (Springer International Publishing) (2015), 109–116.

[33] Cetin S, Özarslan E, Unal G. Elucidating intravoxel geometry in diffusion-MRI: asymmetric orientation distribution functions (AODFs) revealed by a cone model. *International Conference on Medical Image Computing and Computer-Assisted Intervention* (Springer International Publishing) (2015), 231–238.

[34] Budde MD, Frank JA. Neurite beading is sufficient to decrease the apparent diffusion coefficient after ischemic stroke. *Proc Natl Acad Sci U S A* **107** (2010) 14472–7. doi:10.1073/pnas.1004841107.

[35] Press WH, Teukolsky SA, Vetterling WT, Flannery BP. *Numerical Recipes in C: The Art of Scientific Computing* (Cambridge: Cambridge Press) (1992).

[36] Debye P. Zerstreuung der röntgenstrahlen. *Ann Physik* **46** (1915) 809–824.

[37] Glatter O, Kratky O, editors. *Small Angle X-Ray Scattering* (London: Academic Press) (1982).

[38] Feigun LA, Svergun DI. *Structure Analysis by Small-Angle X-Ray and Neutron Scattering* (New York: Springer Science + Business Media) (1987).

[39] des Cloizeaux J. Form factor of an infinite Kratky-Porod chain. *Macromolecules* **6** (1973) 403–407.

[40] Mitra PP, Halperin BI. Effects of finite gradient-pulse widths in pulsed-field-gradient diffusion measurements. *J Magn Reson A* **113** (1995) 94–101.

[41] Neuman CH. Spin echo of spins diffusing in a bounded medium. *J Chem Phys* **60** (1974) 4508–4511.

[42] Baxter JR, Brosamler GA. Energy and the law of the iterated logarithm. *Math Scand* **38** (1976) 115–136.

[43] Özarslan E, Yolcu C, Herberthson M, Westin CF, Knutsson H. Effective potential for magnetic resonance measurements of restricted diffusion. *Front Phys* **5** (2017) 68.

[44] Schoonover C. *Portraits of the Mind* (New York, NY: Abrams) (2010).

[45] Parekh R, Ascoli GA. Quantitative investigations of axonal and dendritic arbors: development, structure, function, and pathology. *Neuroscientist* **21** (2015) 241–54. doi:10.1177/1073858414540216.

[46] Hansen MB, Jespersen SN, Leigland LA, Kroenke CD. Using diffusion anisotropy to characterize neuronal morphology in gray matter: the orientation distribution of axons and dendrites in the NeuroMorpho.org database. *Front Integr Neurosci* **7** (2013) 31. doi:10.3389/fnint.2013.00031.

[47] Jespersen SN, Leigland LA, Cornea A, Kroenke CD. Determination of axonal and dendritic orientation distributions within the developing cerebral cortex by diffusion tensor imaging. *IEEE Trans Med Imaging* **31** (2012) 16–32. doi:10.1109/TMI.2011.2162099.

[48] Najac C, Branzoli F, Ronen I, Valette J. Brain intracellular metabolites are freely diffusing along cell fibers in grey and white matter, as measured by diffusion-weighted MR spectroscopy in the human brain at 7 T. *Brain Struct Funct* **221** (2016) 1245–54. doi:10.1007/s00429-014-0968-5.

[49] Palombo M, Ligneul C, Najac C, Le Douce J, Flament J, Escartin C, et al. New paradigm to assess brain cell morphology by diffusion-weighted MR spectroscopy in vivo. *Proc Natl Acad Sci U S A* **113** (2016) 6671–6. doi:10.1073/pnas.1504327113.

[50] Palombo M, Ligneul C, Valette J. Modeling diffusion of intracellular metabolites in the mouse brain up to very high diffusion-weighting: Diffusion in long fibers (almost) accounts for non-monoexponential attenuation. *Magn Reson Med* **77** (2017) 343–350. doi:10.1002/mrm.26548.

[51] Hilgetag CC, Barbas H. Are there ten times more glia than neurons in the brain? *Brain Struct Funct* **213** (2009) 365–6. doi:10.1007/s00429-009-0202-z.

[52] Purves D, Augustine GJ, Fitzpatrick D, Katz LC, LaMantia AS, McNamara JO, et al., editors. *Neuroscience* (Sunderland, MA: Sinauer Associates), 2 edn. (2001).

[53] Herculano-Houzel S, Lent R. Isotropic fractionator: a simple, rapid method for the quantification of total cell and neuron numbers in the brain. *J Neurosci* **25** (2005) 2518–21. doi:10.1523/JNEUROSCI.4526-04.2005.

[54] Koay CG, Özarslan E, Basser PJ. A signal transformational framework for breaking the noise floor and its applications in MRI. *J Magn Reson* **197** (2009) 108–119. doi:10.1016/j.jmr.2008.11.015.

[55] Özarslan E, Shepherd TM, Koay CG, Blackband SJ, Basser PJ. Temporal scaling characteristics of diffusion as a new MRI contrast: findings in rat hippocampus. *NeuroImage* **60** (2012) 1380–1393. doi:10.1016/j.neuroimage.2012.01.105.

[56] Cajal SR. *Histologie Du Systeme Nerveux De L'Homme Et Des Vertebretes* (Paris: Maloine) (1911).

[57] Van Nguyen D, Grebenkov D, Le Bihan D, Li JR. Numerical study of a cylinder model of the diffusion MRI signal for neuronal dendrite trees. *J Magn Reson* **252** (2015) 103–13. doi:10.1016/j.jmr.2015.01.008.

[58] Palombo M, Gabrielli A, De Santis S, Capuani S. The γ parameter of the stretched-exponential model is influenced by internal gradients: validation in phantoms. *J Magn Reson* **216** (2012) 28–36. doi:10.1016/j.jmr.2011.12.023.

[59] Caporale A, Palombo M, Macaluso E, Guerreri M, Bozzali M, Capuani S. The γ-parameter of anomalous diffusion quantified in human brain by MRI depends on local magnetic susceptibility differences. *NeuroImage* **147** (2017) 619–631. doi:10.1016/j.neuroimage.2016.12.051.

[60] Zheng G, Price WS. Suppression of background gradients in (B_0 gradient-based) NMR diffusion experiments. *Concept Magn Reson A* **30** (2007) 261–277.

[61] Song YQ, Ryu S, Sen PN. Determining multiple length scales in rocks. *Nature* **406** (2000) 178–181. doi:10.1038/35018057.

[62] Álvarez GA, Shemesh N, Frydman L. Internal gradient distributions: A susceptibility-derived tensor delivering morphologies by magnetic resonance. *Sci Rep* **7** (2017) 3311. doi:10.1038/s41598-017-03277-9.

[63] Pathak AP, Ward BD, Schmainda KM. A novel technique for modeling susceptibility-based contrast mechanisms for arbitrary microvascular geometries: the finite perturber method. *NeuroImage* **40** (2008) 1130–43. doi:10.1016/j.neuroimage.2008.01.022.

[64] Kurz FT, Kampf T, Buschle LR, Schlemmer HP, Bendszus M, Heiland S, et al. Generalized moment analysis of magnetic field correlations for accumulations of spherical and cylindrical magnetic perturbers. *Front Phys* **4** (2016) 46.

[65] Tanner JE, Stejskal EO. Restricted self-diffusion of protons in colloidal systems by the pulsed-gradient, spin-echo method. *J Chem Phys* **49** (1968) 1768–1777.

[66] Robertson B. Spin-echo decay of spins diffusing in a bounded region. *Phys Rev* **151** (1966) 273–277.

[67] Barzykin AV. Theory of spin echo in restricted geometries under a step-wise gradient pulse sequence. *J Magn Reson* **139** (1999) 342–353. doi:10.1006/jmre.1999.1778.

[68] Grebenkov DS. NMR survey of reflected Brownian motion. *Rev Mod Phys* **79** (2007) 1077–1137.

[69] Özarslan E, Shemesh N, Basser PJ. A general framework to quantify the effect of restricted diffusion on the NMR signal with applications to double pulsed field gradient NMR experiments. *J Chem Phys* **130** (2009) 104702. doi:10.1063/1.3082078.

[70] Grebenkov DS. Analytical solution for restricted diffusion in circular and spherical layers under inhomogeneous magnetic fields. *J Chem Phys* **128** (2008) 134702. doi:10.1063/1.2841367.

[71] Torrey HC. Bloch equations with diffusion terms. *Phys Rev* **104** (1956) 563–565.

[72] Hörmander L. *The Analysis of Linear Partial Differential Operators I, (Distribution theory and Fourier Analysis)* (Springer-Verlag), 2 edn. (1990).

[73] Yolcu C, Memiç M, Şimşek K, Westin CF, Özarslan E. NMR signal for particles diffusing under potentials: From path integrals and numerical methods to a model of diffusion anisotropy. *Phys Rev E* **93** (2016) 052602.